Grand Unification of AGN and the Accretion and Spin Paradigms

David L. Meier [a,1]

[a] *238-332, Jet Propulsion Laboratory, California Institute of Technology, 4800 Oak Grove Drive, Pasadena, CA 91109*

Abstract

While attempts to unify certain classes of AGN using orientation and environmental effects have been successful, it is widely recognized that intrinsic properties of the accreting black hole system also must play a role in determining the appearance of such an object. In addition to mass and accretion rate, the angular momentum (or spin) of the black hole can play a crucial role in determining the power of a relativistic jet that is generated by magnetohydrodynamic acceleration near the hole. In this paper a scenario is presented, based on accretion theory and recent models of MHD jet production, in which the primary (although not only) parameter differentiating between radio loud and quiet objects is the black hole spin, and that determining quasar vs. radio galaxy is the accretion rate. A surprising number of desirable features result from these simple concepts and the accompanying equations. In addition, there are several testable predictions that can determine whether this grand unification scheme has further merit.

1 Introduction: Heredity *vs.* Environment

Recent attempts to unify certain classes of active galactic nuclei (AGN) using orientation and environmental effects have been rather successful (Orr & Browne 1982) (Antonucci & Miller 1985) (Barthel 1989) (Urry & Padovani 1995) (Wall & Jackson 1999). However, it is widely recognized that intrinsic properties of the accreting black hole systems that are thought to power AGN must also play a role in determining the appearance of these objects. While there is still much to be learned, we now know enough about accretion onto black holes and about the production of jets to begin to develop *grand* schemes that attempt to unify most classes of these objects.

[1] E-mail: dlm@cena.jpl.nasa.gov

In accretion and jet production theory the principal parameters determining the appearance and behavior of the system are the black hole mass M_H, the mass accretion rate $\dot{M}$, and the black hole angular momentum J, expressed in dimensionless form as $m_9 \equiv M_H/10^9\,M_\odot$ (where $M_\odot$ represents one solar mass), $\dot{m} \equiv \dot{M}/\dot{M}_{Edd}$ (where $\dot{M}_{Edd} = 4\pi G M_H/\epsilon\kappa_{es}c = 22\,M_\odot yr^{-1}\,m_9$ is the accretion rate that produces one Eddington luminosity for an efficiency $\epsilon = 0.1$ and electron scattering opacity κ_{es}), and $j \equiv J/J_{max}$ (where $J_{max} = GM_H^2/c$ is the angular momentum of a maximal Kerr black hole). For most AGN and quasar models typical ranges of the parameters are $10^{-3} < m_9 < 10$, $10^{-5} < \dot{m} < 1$, and $0 < j < 1$. While all parameters will affect the properties of an AGN to a certain extent, the purpose here is to identify the principal observable effects of each.

The unification through intrinsic effects discussed here is not meant to replace that which has been accomplished already through extrinsic considerations. Rather, the accreting black hole system should be considered as providing the basic parent ensemble of AGN in which orientation and environmental effects can take place. Pursuant to the anthropomorphological theme of this conference, this paper will deal with the "psychology" of AGN: some traits are inherited from birth (*i.e.*, from the accreting system) and some are a product of the source's environment. Considerations of both types of effects will lead to a better understanding of the life cycles of AGN.

2 The Accretion Paradigm: Effects of Black Hole Mass and Accretion Rate

The accretion paradigm states that most, and perhaps all, AGN are powered by accretion onto a supermassive black hole (see, *e.g.*, Blandford & Rees 1991). Within this model $\dot{m}$ plays the most important role, determining the emission properties, and therefore the appearance, of the central source. Objects with high accretion rate ($\dot{m} \gtrsim 0.1$) appear as an "optical" quasar (of course, equally bright, if not brighter, in X-rays as well), while low sub-Eddington accretion ($\dot{m} \lesssim 10^{-2}$) produces a weak "radio" core with substantially less optical emission. A zero accretion rate produces a "dead" quasar — a black hole detectable only through its gravitational influence on the galactic nucleus. For a given $\dot{m}$ level, the black hole mass determines mainly the luminosity scaling.

2.1 Observational and Theoretical Evidence for the Accretion Paradigm

There is both observational and theoretical evidence for this picture. Based on optical spectra of AGN, Jackson & Wall (1999) identify two classes of object:

Class A (quasars, "N" radio galaxies, Seyfert galaxies) with strong *narrow* emission lines and Class B (most radio galaxies and weak radio cores) with weak or no narrow line emission. Narrow line strength is considered a better parameter than, for example, broad line strength, as it is less affected by orientation effects (see, *e.g.*, Antonucci & Miller 1985). In this scheme Class A objects are identified with high nuclear gas content and, therefore, with high accretion rate, while Class B AGN are identified with low accretion rate. An important point noted by Jackson & Wall is that the Fanaroff & Riley Class I radio sources are an homogeneous class, while FR II sources are not: FR Is are all Class B AGN while most, but not all, FR IIs are Class A. *That is, some FR II sources appear to have powerful jets and yet a rather low accretion rate.*

In addition, in present theories of accretion, a rapidly-accreting supermassive black hole embedded in an elliptical bulge of stars is predicted to appear as a quasar-like object (1-2 orders of magnitude brighter than its host). For $\dot{m} \gtrsim 0.1$ the standard disk models of Shakura & Sunyaev (1973) appear to be most appropriate, with the optical luminosity (integrated disk emission from plasma at a temperature of $< 10^5\,K$) scaling in solar units as

$$L_{acc}^{opt} \;\geq\; 1.7 \times 10^{12} L_{\odot}\, m_9^{1.27} \left(\frac{\dot{m}}{0.1}\right)^{0.6} \tag{1}$$

If the black hole mass is directly related to galactic bulge luminosity, *i.e.*, $L_{gal}^{opt} \approx 2.4 \times 10^{10} L_{\odot}\, m_9^{0.8}$, as suggested by Kormendy & Richstone (1995), then the ratio of accretion disk to bulge luminosity is

$$\frac{L_{acc}^{opt}}{L_{gal}^{opt}} \;>\; 68 m_9^{0.47} \tag{2}$$

for $\dot{m} > 0.1$. On the other hand, a drop in accretion rate well below this value produces a much fainter "advection-dominated" (Narayan *et al.* 1998) accretion disk with bolometric luminosity dropping as $L_{acc}^{bol} \propto \dot{m}^2$, and optical luminosity dropping even faster than that. (The exact accretion rate at which this drop-off occurs [$\dot{m}_{cr} \sim \alpha^2$] varies steeply with the value of the viscosity parameter α, which is usually taken to be ~ 0.3 for ADAF models.) Such disks are geometrically thick, optically thin, and emit mainly nonthermal radio emission. For the remainder of this paper, we will take $\dot{m} = 0.1$ to be typical of Class A quasar-like objects and $\dot{m} = 0.01$ to be typical of Class B radio cores.

2.2 Observations Explained

Several interesting corollaries immediately follow from this picture. For black holes in elliptical galaxies, only dwarf ellipticals are brighter than their central quasar ($L_{acc}^{opt} < L_{gal}^{opt}$ when $m_9 < 10^{-4}$, or when the galaxy magnitude is $\mathcal{M}_{gal}^{opt} > -13$). However, for holes in spiral galaxies, where the optical luminosity is dominated by a stellar disk of luminosity $\sim 2 \times 10^{10} L_{\odot}$, the object will appear as a Seyfert galaxy rather than a quasar ($L_{gal}^{opt} > L_{acc}^{opt}$) for black holes of rather high mass ($m_9 < 0.03$ or $M_H < 3 \times 10^7 M_{\odot}$). The simple accretion paradigm, therefore, accounts for several of the basic *optical* properties of Seyfert, radio galaxy, and quasar (parent) populations.

3 The Spin Paradigm: Effects of Black Hole Rotation

The spin paradigm states that, to first order, it is the normalized black hole angular momentum j that determines whether or not a strong radio jet is produced (Wilson & Colbert 1995) (Blandford 1999). If correct, this hypothesis has significant implications for how we should view the jets and lobes in radio sources: the jet radio and kinetic energy comes directly from the rotational energy of a (perhaps formerly) spinning black hole. *Radio sources are not powered (directly) by accretion.*

3.1 Theoretical Arguments for the Spin Paradigm

There is significant theoretical basis for this paradigm as well. Several models of relativistic jet formation (Blandford & Znajek 1977) (Punsly & Coroniti 1990) indicate that the jet power should increase as the square of the black hole angular momentum

$$L_{jet} \;=\; 10^{48} \mathrm{erg\,s^{-1}} \left(\frac{B_p}{10^5 G} \right)^2 m_9^2 \, j^2 \tag{3}$$

where B_p is the strength of the poloidal (vertical/radial) magnetic field threading the ergospheric and horizon region of the rotating hole. In this model rotational energy is extracted via a Penrose-like process: the frame-dragged accretion disk is coupled to plasma above and outside the ergosphere via the poloidal magnetic field; some plasma is pinched and accelerated upward while some disk material is diverted into negative energy (retrograde) orbits inside the ergosphere, removing some of the hole's rotational energy. The key parameter determining the efficiency of this process is the strength of the poloidal

magnetic field. The standard approach (*e.g.,* Moderski & Sikora 1996) to estimating B_p is to set it equal to B_ϕ, the dominant azimuthal magnetic field component given by the disk structure equations, yielding

$$L_{jet,B} = 2 \times 10^{45} \mathrm{erg\,s^{-1}}\, m_9 \left(\frac{\dot{m}}{0.01}\right) j^2 \tag{4}$$

$$L_{jet,A} = 3 \times 10^{49} \mathrm{erg\,s^{-1}}\, m_9^{1.1} \left(\frac{\dot{m}}{0.1}\right)^{0.8} j^2 \tag{5}$$

for Class B (radio galaxy/ADAF) and Class A (quasar/standard disk) objects, respectively. Note that, while the jet is not accretion-powered in this model, the efficiency of extraction is still essentially linear in $\dot{m}$.

Livio, *et al.* (1999) have pointed out that taking $B_p \approx B_\phi$ may greatly overestimate the jet power from this process. Using dynamo arguments they propose that a more realistic estimate for the equilibrium poloidal magnetic field is

$$B_p \approx (H/R)\, B_\phi \tag{6}$$

where (H/R) is the ratio of disk half-thickness to radius in the jet acceleration region. For *thin* disks this yields a jet power of only $L_{jet} = 4 \times 10^{44} \mathrm{erg\,s^{-1}}\, m_9^{1.1}\, (\dot{m}/0.1)^{1.2}\, j^2$ — less than the observed *radio* power of the strongest sources and much less than their inferred total jet power (see Bicknell, these proceedings, and Bicknell 1995). However, there are several reasons for believing that even with equation (6) the field still can be quite large in many cases, and the jet power still comparable to equations (4) and (5). Firstly, for advective disks (both the accretion-starved kind [$\dot{m} << 1$] and the super-Eddington kind [$\dot{m} \gtrsim 1$]) the disk is geometrically thick ($H/R \sim 1$), yielding $B_p \approx B_\phi$ even within the dynamo argument. Thick disks also can occur for an even broader range of accretion rate when the hole and disk spin axes are misaligned: because of the Lens-Thirring effect, the gas follows inclined orbits that do not close, creating shocks and dissipation that bloats the disk into a quasi-spherical, inhomogeneous inflow (Blandford 1994). Furthermore, even when $H << R$, inside the last stable orbit (or in any other region of the disk where the infall velocity suddenly approaches the free-fall speed) conservation of mass will cause a drop in density and pressure. The toroidal field may then be dynamically important, buckling upward out of the plunging accretion flow, resulting in B_p being comparable to B_ϕ (Krolik 1999).

Figure 1 summarizes the main features of the accretion and spin paradigms and shows the four possible combinations of high and low accretion rate and black hole spin. It is proposed that these states correspond to different radio loud and quiet quasars and galaxies. In the figure poloidal magnetic field strengths are estimated from equation (6), but (H/R) is of order unity for

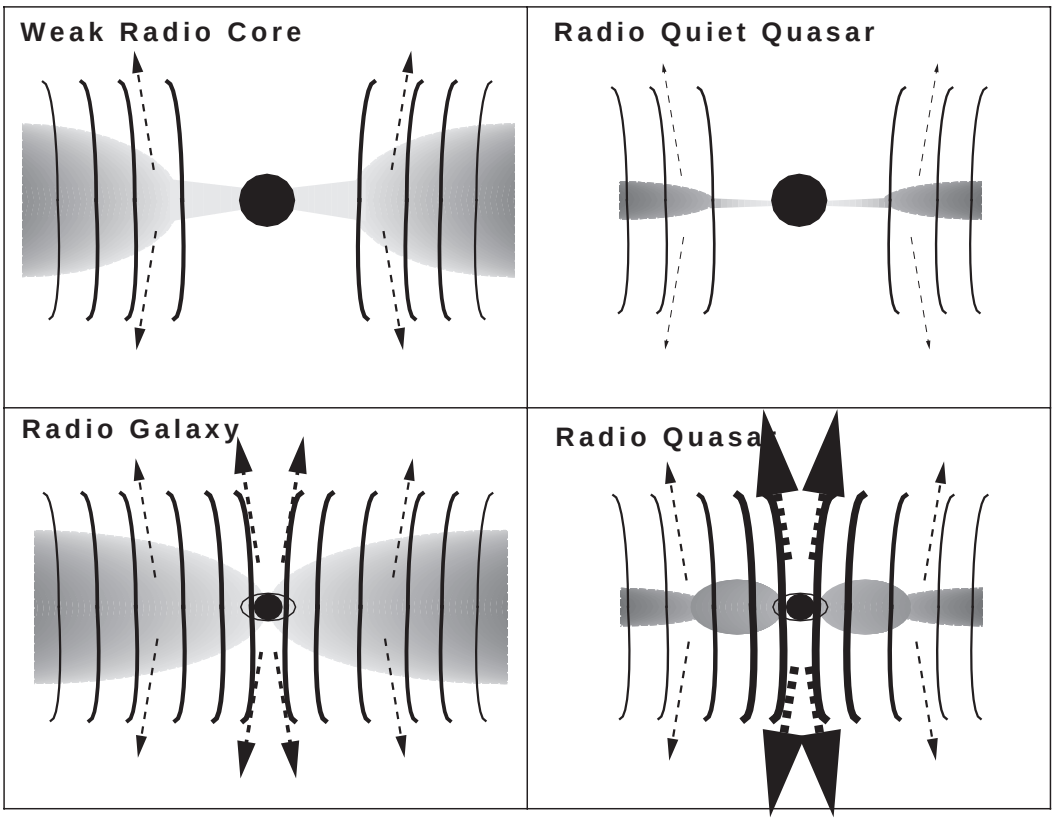

Fig. 1. Schematic representation of four possible combinations of $\dot{m}$ and j, drawn roughly to scale. The horizon interior to the hole is black, while the boundary of the ergosphere (the "static limit") is represented by an ellipse 0.5×1.0 Schwarzschild radius in size. Top panels depict non-rotating, Schwarzschild holes ($j \to 0$), bottom panels Kerr holes ($j \to 1$). Left panels show low accretion rate (ADAF) tori, right panels high accretion rate standard disk models. However, in the lower right panel the region of the disk experiencing significant frame dragging is bloated (*c.f.* Blandford 1994). Widths of poloidal magnetic field lines and jet arrows are proportional to the logarithm of their strength.

the low $\dot{m}$ cases, and also for the high $\dot{m}$ Kerr case due to Lens-Thirring bloating of the inner disk. Otherwise (H/R) is calculated from the electron scattering/gas pressure disk model of Shakura & Sunyaev (1973), and disk field strengths are computed from that paper or from Narayan *et al.* (1998), as appropriate. The logarithms of the resulting poloidal field strengths, and corresponding jet powers, are represented as field line and jet arrow widths. In the Kerr cases, the inner disk magnetic field is significantly enhanced over the Schwarzschild cases, due in part to the smaller last stable orbit (flux conservation) and in part to the large (H/R) of the bloated disks. The high accretion rate, Schwarzschild case has the smallest field — and the weakest jet — because the disk is thin, the last stable orbit is relatively large, and the Keplerian rotation rate of the field there is much smaller than it would be in a Kerr hole ergosphere. Enhancement of the poloidal field due to the

buoyancy process suggested by Krolik (1999) is ignored here because we find it not to be a factor in the simulations discussed below. If it were important, then the grand scheme proposed here would have to be re-evaluated, as the effect could produce strong jets (up to the accretion luminosity in power) even in the plunging region of Schwarzschild holes. Then even the latter would be expected to be radio loud as well ($L_{jet} \sim 10^{43-46}\mathrm{erg\,s^{-1}}$).

3.2 General Relativistic Simulations of Magnetized Disks in Kerr Geometry

Recent work by S. Koide, the author, and K. Shibata and T. Kudoh on general relativistic simulations of the accretion of magnetized material by black holes is beginning to provide a clearer picture of the development and evolution of a black hole magnetosphere and the resulting jet. Initial indications are that rapid rotation of the black hole *and* rapid infall of the magnetized plasma into this rotating spacetime both contribute to powerful, collimated, relativistic jet outflows. We find no evidence for buoyant poloidal field enhancement in the plunging region and, therefore, no reason to expect Schwarzschild holes to have a jet any more powerful than that estimated in Figure 1.

Figure 2 shows the initial and final state of a Kerr ($j = 0.95$) black hole simulation with a weak ($V_A \equiv B_p/\sqrt{4\pi\rho_{disk}} = 0.01c$) magnetic field and an inner edge at $R_{in} = 4.5\,GM_H/c^2$. For more details see Koide *et al.* (1999a). In this first simulation the disk was *non-rotating*, and so began to free-fall into the ergosphere (at $R_{ergo} = 2GM_H/c^2$) as the calculation proceeded. As with other MHD disk simulations (Kudoh & Shibata 1995) (Ustyugova *et al.* 1995) (Ouyed & Pudritz 1997) (Meier *et al.* 1997), the field lines were wound up by differential rotation and a hollow jet of material was ejected along the poloidal field lines by the $\mathbf{J} \times \mathbf{B}$ forces; here the jet velocity was rather relativistic ($v_{jet} \sim 0.93c$ or $\Gamma \sim 2.7$). However, as the disk was initially non-rotating, all the action was due to the differential dragging of frames by the rotating black hole. Little or no jet energy was derived from the binding energy of the accreting material or its Keplerian rotation.

As a control experiment, the same simulation was also run with a Schwarzschild ($j = 0$) hole. The collapse developed a splash outflow due to tidal focusing and shocking of the inflowing disk, but no collimated MHD jet occurred.

We also studied counter-rotating and co-rotating Keplerian disks with otherwise similar initial parameters (Koide *et al.* 1999b). The counter-rotating case behaved nearly identically to the non-rotating case: because the last stable retrograde orbit is at $R_{ms} = 9GM_H/c^2$, the disk began to spiral rapidly into the ergosphere, ejecting a strong, black-hole-spin-driven MHD jet. On the other hand, for prograde orbits $R_{ms} = GM_H/c^2$, so the co-rotating disk

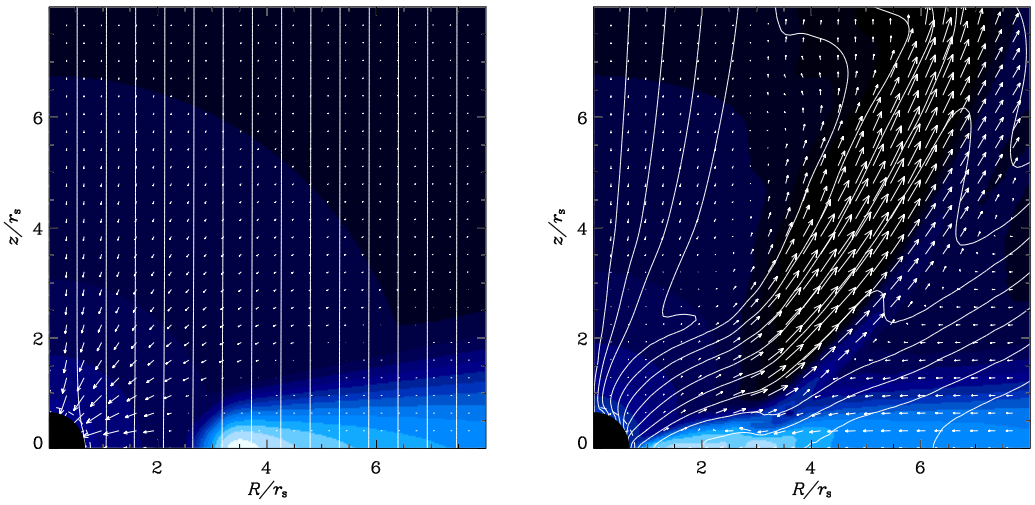

Fig. 2. General relativistic simulation of a magnetized flow accreting onto a Kerr black hole (after Koide *et al.* 1999a). Left panel shows one quadrant of the initial model with the $j = 0.95$ hole at lower left, freely-falling corona, and non-rotating disk. The hole rotation axis (Z) is along the left edge. The initial magnetic field (vertical lines) is weak compared to the matter rest energy density ($V_A = 0.01c$). Right panel shows final model at $t = 130\,GM_H/c^3$. Some of the disk and corona have been accreted into the hole, threading the ergosphere and horizon with magnetic field lines that develop a significant radial component, and hence an azimuthal component as well, due to differential frame dragging. The resulting jet outflow is accelerated by $\mathbf{J} \times \mathbf{B}$ forces to a Lorentz factor of 2.7.

was stable, accreting on a slow secular time scale. At the end of the calculation ($t_{max} = 94\,GM_H/c^3$), when the simulation had to be stopped because of numerical problems, the disk had not yet accreted into the ergosphere and had produced only a weak MHD jet. Future evolution of this case is still uncertain. The Keplerian Schwarzschild case was previously reported by Koide *et al.* (1998) and developed a moderate sub-relativistic MHD jet similar to the aforementioned simulations of magnetized Keplerian flows around normal stars, plus a pressure-driven splash outflow internal to the MHD jet.

In the Kerr cases we see significant magnetic field enhancement over the Schwarzschild cases due to compression and differential frame dragging. It is this increase that is responsible for the powerful jets ejected from near the horizon. In the Schwarzschild cases, on the other hand, — particularly in the Keplerian disk case in Koide *et al.* (1998) — we do *not* see any MHD jet ejected from well inside R_{ms}. That is, we do not see any increase in jet power that could be attributed to buoyant enhancement of the poloidal field in the plunging region. While there is a jet ejected from inside the last stable orbit, it is pressure-driven by a focusing shock that develops in the accretion flow. The magnetically-driven jet that does develop in the Schwarzschild case emanates

from near the last stable orbit as expected, not well inside it. It is therefore concluded that a powerful MHD jet will be produced near the horizon if and only if the hole is rotating rapidly.

3.3 Observational Advantages of the Spin Paradigm

There are several observational advantages to the spin paradigm for AGN. It lifts the degeneracy of accretion onto black holes and explains the difference between radio loud and radio quiet objects: a given central source type (m_9, $\dot{m}$) can have a powerful jet ($j \to 1$) or little or no jet at all ($j \to 0$). Maximal Kerr holes produce powerful radio sources while Schwarzschild holes produce "radio quiet" objects. Even with only modest efficiency in converting the jet into particles and fields, the spent rotational energy of a black hole ($E_{rot} \approx 10^{62}\mathrm{erg}\, m_9\, j^2$) can easily account for the observed energy in the lobes of the most powerful sources (DeYoung 1975). Taking the FR I/II break to occur at a jet power of $10^{44}\mathrm{erg}\, s^{-1}$ for a $10^9 M_\odot$ hole (using a Bicknell flux conversion factor of $\kappa_\nu = 10^{-11}\mathrm{Hz}^{-1}$) equations (4) and (5) predict correctly that radio quasars (Class A, $\dot{m} = 0.1$, $j = 0.01$-1.0) will be predominantly FR II sources ($10^{45-49}\mathrm{erg\,s}^{-1}$), low-spin radio galaxies (Class B, $\dot{m} = 0.01$, $j = 0.01$-0.1) will be FR I sources ($10^{41-43}\mathrm{erg\,s}^{-1}$), but there should be a population of Class B sources with low accretion rate and high black hole spin ($\dot{m} = 0.01$, $j = 0.1$-1.0) that produce some FR II sources without central quasars ($10^{43-45}\mathrm{erg\,s}^{-1}$). These are the Class B FR II sources noted by Jackson & Wall (1999).

The spin paradigm even offers an explanation for why present-day giant radio sources occur only in elliptical galaxies and why the distribution of optically-selected quasars may be bi-modal in radio power. The e-folding spindown time (E_{rot}/L_{jet}) is very short — much shorter than a cosmic evolutionary time

$$\tau_{spindown} \approx 10^6\mathrm{yr} \left(\frac{\dot{m}}{0.1}\right)^{-0.8} \left(\frac{\zeta_{duty}}{0.1}\right)^{-1} \tag{7}$$

even with a jet active duty cycle of only 10%. As a result, *all AGN should be radio quiet at the present epoch*, their black holes having spun down when the universe was very young. In order to continually produce radio sources up to the present epoch, there must be periodic input of significant amounts of angular momentum from accreting stars and gas, or from a merger with another supermassive black hole (see also Wilson & Colbert 1995). Such activity is triggered most easily by violent events such as galaxy mergers. Since only elliptical galaxies undergo significant mergers (the merging process is believed to be *responsible* for their elliptical shape), *only ellipticals are expected to be giant radio sources in the present epoch.* With little merger activity, spiral

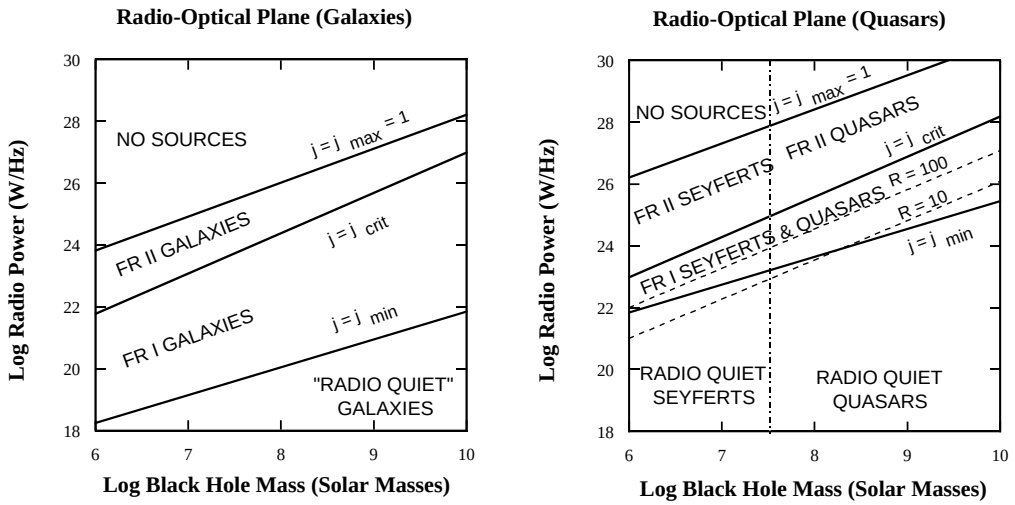

Fig. 3. Example of a grand unification scheme (after Meier 1999). Left panel shows Class B objects (*e.g.*, radio galaxies; $\dot{m} = 0.01$), right panel Class A objects (*e.g.*, quasars; $\dot{m} = 0.1$). Lines dividing the radio-optical planes are discussed in the text.

galaxies are expected to be relatively radio quiet. Since merging and non-merging galaxies will fuel and re-kindle their black hole's spin in very different ways, bi-modality in the radio luminosity distribution is to be expected.

4 An Example Grand Unification Scheme — Observational Predictions

Figure 3 shows two radio-optical planes for Class A and Class B objects in an example grand unification scheme (after Meier 1999). These figures are to be compared with observed radio-optical planes like that of Ledlow & Owen (1996). As the optical luminosity of the galaxy or quasar scales with black hole mass in both cases, the horizontal axis is M_H in both. The vertical axis is the observed radio power using the Bicknell factor κ_ν to convert L_{jet} to P^{rad}. The curves separate the plane into several different black hole spin states: NO sources ($j > 1$ is not allowed); FR II sources ($j_{crit} < j < 1$), FR I sources ($j_{min} < j < j_{crit}$), and radio quiet objects ($j < j_{min}$). For j_{crit} we have used here the generalized magnetic switch of Meier (1999), but Bicknell's FR I/II transonic condition could be substituted. For j_{min} we have chosen the point where the predicted black hole MHD power in equation (5) equals the thin disk MHD power with $B_p = (H/R)B_\phi$. Other observational definitions of radio quietness (using the radio-optical flux ratio) are shown.

This grand unification scheme makes some interesting predictions. There should

be a population of sources corresponding to FR I quasars (high $\dot{m}$, low j). These were formerly FR II sources, but their holes have since spun down. However, the spindown time for Class A sources is so short (equation 7) that it is likely that the FR II hot spots will still be radiating as the source goes through the FR I phase. Such hybrid FR II sources could be identified by *young* diffuse emission or "bridges" between the radio core and the hot spots. The FR IIa quasars identified by R. Daly (these proceedings) are candidates for such sources; the FR IIa/IIb transition also appears to occur near the $j = j_{crit}$ line in Figure 3b.

There also should be a population of high redshift, faint sub-mJy FR I and II radio sources associated with spiral galaxies or pre-spiral bulges ($M_H < 10^7 M_\odot$). If the accretion rate was high at that time — the most likely case in the early universe — then these may appear as optically faint radio quasars ($L^{opt} \lesssim 10^{43} \mathrm{erg\,s^{-1}}$, $P^{rad} \lesssim 10^{23-27} \mathrm{W\,Hz^{-1}}$). Their numbers should be a significant fraction of the present-day spiral population, exceeding the contribution of quasars residing in elliptical galaxies alone.

5 Discussion and Conclusions

Considerably more theoretical and observational work is needed to further refine and test grand schemes of this type, including more detailed simulations of Kerr black hole magnetospheres and a better understanding of the structure and strength of the magnetic field near rotating (and non-rotating) holes. Furthermore, any complete grand scheme must explain, from first principles, how the fundamental features of optical quasar spectra ("nonthermal" continuum, broad and narrow lines) are produced and how accreting black holes should look at near-Eddington and super-Eddington accretion rates.

On the observational side, good methods of estimating the central accretion rate and black hole spin are needed to locate each source in (M_H, $\dot{M}$, J)-space. As has been done in the past for stars and galaxies, when relations between fundamental parameters and observable properties are understood, an overall picture of how seemingly disparate objects are related begins to emerge.

Acknowledgements

The author is grateful to S. Koide for discussions and for permission to use Figure 2. This research was carried out at the Jet Propulsion Laboratory, California Institute of Technology, under contract to NASA.

References

Antonucci, R. & Miller, J. 1985, ApJ, 297, 621.

Barthel, P. D. 1989, ApJ, 336, 606.

Bicknell, G. V. 1995, ApJS, 101, 29.

Blandford, R. D. 1994, in *The Physics of Active Galaxies*, proceedings of ASP Conf. Ser., Vol. 54, ed. G. V. Bicknell, M. A. Dopita, & P. J. Quinn, p. 23.

Blandford, R. D. 1999, in *Astrophysical Disks*, proceedings of ASP Conf. Ser., Vol. 160, ed. J. A. Sellwood and J. J. Goodman.

Blandford, R. D. & Rees, M. J. 1991, in *Testing the AGN Paradigm*, proceedings of AIP Conference #254, ed. S. S. Holt, S. G. Neff, & C. M. Urry, p. 3.

Blandford, R. D. & Znajek, R. 1977, MNRAS, 179, 433.

DeYoung, D. 1976, ARAA, 14, 447.

Jackson, C. A. & Wall, J. V. 1999, MNRAS, 304, 160.

Koide, S., Shibata, K., & Kudoh, T. 1998, ApJL, 495, L63.

Koide, S., Meier, D. L., Shibata, K., & Kudoh, T. 1999a, preprint, astro-ph/9907435, to appear in the 19th Texas Symposium on Relativistic Astrophysics.

Koide, S., Meier, D. L., Shibata, K., & Kudoh, T. 1999b, preprint submitted to ApJ, astro-ph/9907435.

Kormendy, J. & Richstone, D. 1995, Ann. Rev. Astr. Ap., 33, 581.

Krolik, J. H. 1999, ApJL, 515, L73.

Kudoh, T. & Shibata, K. 1995, ApJ, 452, L41.

Ledlow, M. J. & Owen, F. N. 1996, AJ, 112, 9.

Livio, M., Ogilvie, G. I., & Pringle, J. E. 1999, ApJ, 512, 100.

Meier, D. L. 1999, ApJ, 522, in press.

Meier, D. L., Edgington, S., Godon, P., Payne, D. G., & Lind, K. R. 1997, Nature, 388, 350.

Moderski, R. & Sikora, M. 1996, MNRAS, 283, 854.

Narayan, R., Mahadevan, R., & Quataert, E. 1998, preprint, astro-ph/9803141, to appear in *The Theory of Black Hole Accretion Disks*, eds. M. A. Abramowicz, G. Bjornsson, and J. E. Pringle.

Orr, M. J. L. & Browne, I. W. A. 1982, MNRAS, 200, 1067.

Ouyed, R. & Pudritz, R. E. 1997, ApJ, 482, 712.

Punsly, B. & Coroniti, F. V. 1990a, ApJ, 350, 518.

Shakura, N. I. & Sunyaev, R. A. 1973, Astron. Astroph., 24, 337.

Urry, C. M., & Padovani, P. 1995, PASP, 107, 803.

Ustyugova, G. V., Koldoba, A. V., Romanova, M. M., Chechetkin, V. M., & Lovelace, R. V. E. 1995, ApJ, 429, L39.

Wall, J. V. & Jackson, C. A. 1999, preprint, astro-ph/9907441, to appear in *Building the Galaxies: from the Primordial Universe to the Present Day*, proceedings of the XIX Moriond Astrophysics meeting.

Wilson, A. S. & Colbert, E. J. M. 1995, ApJ, 438, 62.

Q: P. Barthel: The PG (Palomar-Green) QSOs show bi-modality in radio loudness (Kellermann *et al.* 1989, AJ, 98, 1195). If this holds up, will you be worried? That is to say, would you expect a continuous distribution of radio loudness in optically-selected QSOs?

A: D. L. Meier: No, I wouldn't be worried; in fact, bi-modality is to be expected in a scenario where one population of objects is fueled by mergers (ellipticals) and one is fueled by mostly internal processes within the galaxy (spirals). One would expect these to have very different distributions in radio power. These issues also have been discussed by Wilson & Colbert (1995).

Q: D. E. Harris: Does your code accelerate particles (and if so, which), or is Poynting flux the primary output?

A: D. L. Meier: The general relativistic Kerr code of Dr. Koide is an ideal magnetohydrodynamic code. There is only a single (fully ionized) fluid that is accelerated by the $\mathbf{J} \times \mathbf{B}$ force. We do not compute a particle spectrum, unlike T. Jones and I. Tregillis, who will discuss their jet propagation simulations later in the meeting.